

Bridged Denoising Diffusion in Ultra-Low Field MRI Enhancement Challenge

Baris Imre¹  , Chinmay Rao¹, Aram Salehi^{2,3}, Marius Staring¹, Efe Ilicak¹

¹ Division of Image Processing, Department of Radiology, Leiden University Medical Center, Leiden, The Netherlands

² Department of Human Genetics, Radboud University Medical Center, Nijmegen, The Netherlands

³ Department of Radiology, Leiden University Medical Center, Leiden, The Netherlands

Abstract. Low-field MRI offers a cost-effective and portable alternative to conventional high-field systems, but its clinical use is limited by reduced image quality. Recent advancements in deep learning have aimed to enhance low-field scans, including approaches based on GANs, stochastic quality transfer, and denoising diffusion models. In this paper, we introduce a bridged denoising diffusion model that explicitly aligns the latent spaces of low- and high-field MR images through a learned bridging model. At a predefined timestep in the diffusion process, a bridge network translates the noisy low-field representation into the high-field domain, enabling the downstream diffusion model, trained solely on high-field data, to generate high-field-like images. The proposed method is trained on paired 3T and 0.64 mT scans across multiple contrasts, based on the "Enhancing Ultra-Low-Field MRI with Paired High-Field MRI Comparisons for Brain Imaging" challenge. On the hidden validation set, our method achieved an SSIM of 0.779 and a PSNR of 22.85 dB, outperforming alternative configurations in ablation experiments. We show that our model can significantly enhance low-field images.

Keywords: Low-field enhancement, MRI enhancement, Denoising diffusion

1 Introduction

MRI is a cornerstone imaging modality due to its excellent soft tissue contrast and non-ionizing nature [1]. It offers versatile imaging capabilities across multiple anatomical regions and clinical indications, while being an extremely valuable research tool. Despite its advantages, conventional MRI systems are often expensive, immobile, and require significant operational infrastructure. The limited accessibility of conventional MR scanners is primarily due to their high costs. [2, 3]

To address these, low-field (<0.1 T) MR scanners have recently seen a resurgence in interest as a more accessible and cost-effective alternative [4]. With

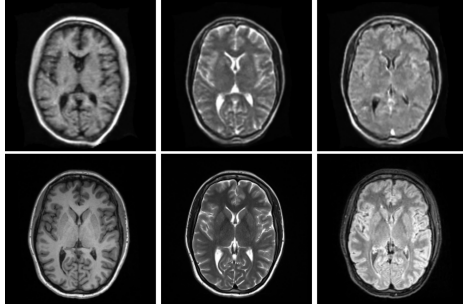


Fig. 1. A comparison of paired 3T and 0.64 mT MR images in three different contrasts. From left to right: T1-w, T2-w, FLAIR. Top row: low-field, bottom row: high-field.

portable designs based on permanent magnets and lower infrastructural requirements, these devices can be deployed outside conventional MRI suites, such as for point-of-care imaging [5, 6]. While recent works have demonstrated the feasibility of these systems in detecting numerous conditions [7–9], obtaining diagnostic-quality images with these systems remains a challenge [10].

Approaches to low-field MRI enhancement have included image-to-image translation methods based on GANs, which aim to synthesize high-field quality images from paired low-field inputs [11]. While effective, such models can suffer from instability and hallucinated features. Other efforts have explored alternative strategies such as stochastic image quality transfer, which avoids adversarial training by learning uncertainty-aware mappings between low and high-field images [12]. In parallel, denoising diffusion models have gained momentum in the MRI community, particularly in the context of accelerated MRI reconstruction [13, 14]. Although originally applied to reconstruct undersampled k-space acquisitions, the same modeling principles have been adapted to the low-field enhancement setting with promising results as well [15, 16].

In this paper, we propose a bridged denoising diffusion model and training scheme to enhance low-field images to their paired high-field counterparts. We describe our methodology in depth and present results on a challenge setting.

2 Materials and Methods

Figure 2 shows an overview of the bridged denoising diffusion model that we propose. Our method has two main components, namely the bridge and the denoising diffusion. In both of the components, we combine the three contrasts of each sample along the channel dimension, promoting the networks to learn and cross reference using all three contrasts.

2.1 Dataset and task

We conduct all of our experiments with a dataset of 50 paired 3D MR images with an addition of a validation and test set that is withheld from us. All scans

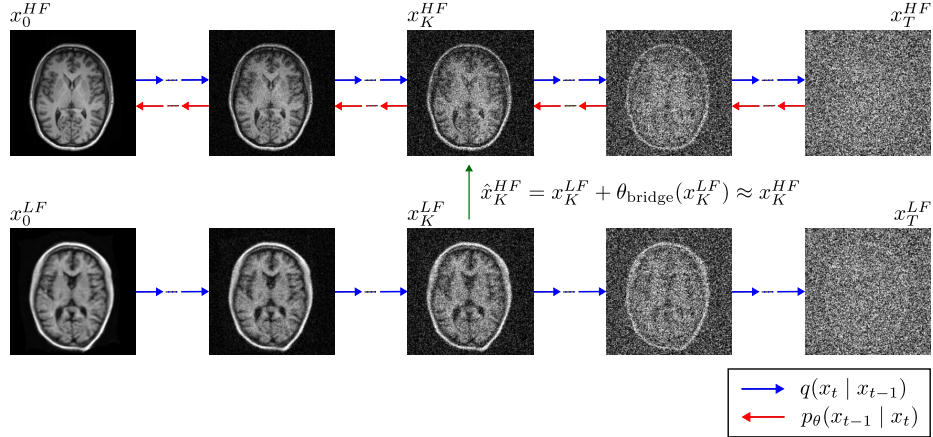


Fig. 2. An overview of the bridged denoising diffusion model for low-field MR enhancement. Two diffusion tracks are presented. On top: high-field, below: low-field. The timesteps from left to right range from $t = 0$ to $t = T$. The bridging step, parameterized by the bridge network ϕ_{bridge} bridges the gap between x_{LF} and x_{HF} at $t = K$.

are resampled to an isotropic resolution of 1 mm^3 . The pairs consist of 3T and 0.64mT MR scans in T1-w, T2-w, and FLAIR contrasts. All scans are co-registered. The challenge data is acquired using a Siemens Biograph mMR (3T) scanner and a Hyperfine Swoop (64mT) scanner. An example is presented in Section 1. We measure the average SSIM [17] index and the PSNR of the paired samples as 0.547 and 17.35 dB respectively. The enhancement task is therefore defined as producing pseudo high-field samples that score higher.

2.2 Denoising diffusion

Denoising diffusion models are defined with the forward operator as defined by Ho et al. [18]:

$$q(x_t | x_0) = \mathcal{N}(x_t; \sqrt{\bar{\alpha}_t} x_0, (1 - \bar{\alpha}_t) \mathbf{I}) \quad (1)$$

Given the clean starting sample x_0 , we derive a noisy version x_t at timestep t with the noise coefficient $\bar{\alpha}_t$ where $\bar{\alpha}_t = \prod_{s=1}^t \alpha_s$ and $\alpha_s = 1 - \beta_s$ and β_s is a predefined noise schedule. This results in Gaussian noise being added on top of the clean sample gradually. We use a cosine based noise schedule. The objective of the denoising diffusion network is to reverse this process by predicting the noise at the given timestep and denoise with the following process:

$$p_\theta(x_{t-1} | x_t) = \mathcal{N}(x_{t-1}; \mu_\theta(x_t, t), \sigma_t^2 \mathbf{I}) \quad (2)$$

defining,

$$\mu_\theta(x_t, t) = \frac{1}{\sqrt{\alpha_t}} \left(x_t - \frac{\beta_t}{\sqrt{1 - \bar{\alpha}_t}} \epsilon_\theta(x_t, t) \right) \quad (3)$$

The neural network ϵ_θ , with its output $\epsilon_\theta(x_t, t)$, is conditioned by the noisy image and the timestep. The training objective is defined as the negative log likelihood of the Gaussian noise prediction and sample, which reduces to an ℓ_2 norm for Gaussian distributions. We define this training objective, hence loss function as $\mathcal{L}_{\text{noise}}$ such that:

$$\mathcal{L}_{\text{noise}} = \mathbb{E}_{t, x_0, \epsilon} \left[\left\| \epsilon - \epsilon_\theta(\sqrt{\bar{\alpha}_t} x_0 + \sqrt{1 - \bar{\alpha}_t} \epsilon, t) \right\|^2 \right] \quad (4)$$

Additionally, we optimize the denoised output $\mu_\theta(x_t, t)$ with two extra terms. One loss term is based on the SSIM index, and the other is an edge-aware loss function, $\mathcal{L}_{\text{sobel}}$, derived from the Sobel operator [19] and extended for 3D inputs. Given the predicted denoised output \hat{x}_0 and the sample x_0 we convolve with the Sobel kernels (S) along each spatial axis to calculate gradient outputs.

$$G_x = S_x * x, G_y = S_y * x, G_z = S_z * x \quad (5)$$

Here, $*$ denotes 3D convolution, and $S_x, S_y, S_z \in \mathbb{R}^{3 \times 3 \times 3}$ are discrete 3D Sobel kernels that approximate the partial derivatives of the image along the x, y, and z axes. The gradient magnitudes are then approximated and combined:

$$\nabla x \approx \tanh(\sqrt{G_x^2 + G_y^2 + G_z^2}) \quad (6)$$

We use the tanh non-linearity to bound the gradients. We calculate the Sobel loss as:

$$\mathcal{L}_{\text{sobel}} = \|\nabla \hat{x}_0 - \nabla x_0\| \quad (7)$$

2.3 Bridging network

At a predefined timestep K in the diffusion process, we perform a cross-domain transition from the noisy low-field sample x_K^{LF} to its high-field counterpart x_K^{HF} . While both are noised representations of paired scans, we observe a substantial mismatch in their latent distributions at this stage similar to Zhao et al. [20]. This discrepancy poses a challenge for the denoising process, which is trained solely on the high-field domain and expects inputs to lie within its data manifold.

To address this issue, we propose a dedicated bridge network that learns to translate x_K^{LF} into an intermediate representation that better aligns with the latent space of x_K^{HF} . This network is trained exclusively on noised paired samples and optimized to minimize the distance between its output and the corresponding high-field sample at timestep K . By explicitly modeling the domain gap at the noisy level, the bridge facilitates a smoother transition and enables the diffusion model to operate effectively in generating enhanced high-field-like outputs from low-field inputs.

We define the bridge network with parameters ϕ_{bridge} , which takes the noisy low-field input at timestep K , x_K^{LF} , and produces an improved latent representation aligned with the high-field domain:

$$\hat{x}_K^{HF} = x_K^{LF} + \phi_{\text{bridge}}(x_K^{LF}) \quad (8)$$

To train this network, we use the following loss terms. First, we enforce latent alignment by minimizing the ℓ_2 distance between the predicted representation \hat{x}_K^{HF} and the true high-field sample x_K^{HF} at the same timestep. Second, we leverage the fact that x_K^{HF} is constructed by adding Gaussian noise ϵ_K to the clean high-field image x_0^{HF} . By subtracting the same noise from the predicted representation \hat{x}_K^{HF} , we recover an estimate of the clean high-field image, \hat{x}_0^{HF} . We then introduce an additional ℓ_2 loss term between \hat{x}_0^{HF} and the ground truth x_0^{HF} to guide the bridge network toward producing representations more suitable to denoising. Finally, we regularize the bridge network with a third loss term that enforces a form of self-identity. After each standard training step, we input the high-field sample into the bridge and encourage the network to produce a minimal residual. Specifically, we use the high-field label as input and minimize the following identity loss:

$$\mathcal{L}_{\text{identity}} = \|x_K^{HF} - (x_K^{HF} + \phi_{\text{bridge}}(x_K^{HF}))\|_2^2 \quad (9)$$

This term ensures that the bridge network does not unnecessarily change inputs already aligned with the high-field distribution, promoting stability and preventing overcorrection.

2.4 Inference

In addition to the conventional denoising diffusion inference algorithm, we find adding intermediate steps that further "correct" at each timestep, inspired from the Predictor-Corrector (PC) sampling of Chung et al. [21], increases denoising efficiency. We use the following algorithm. At each timestep, instead of denoising and adding the noise for the next timestep, we iterate on the same noise level with the same noise sample.

We define two operators to simulate the forward and reverse diffusion processes to simplify the pseudo-code given later in this subsection. **AddNoise** adds noise to a clean sample x_0 at timestep t . **RemoveNoise** denoises a noisy sample x_t at timestep t using the predicted noise $\epsilon_\theta(x_t, t)$:

$$\text{AddNoise}(x, \epsilon, t) = \sqrt{\bar{\alpha}_t} \cdot x + \sqrt{1 - \bar{\alpha}_t} \cdot \epsilon \quad (10)$$

$$\text{RemoveNoise}(x_t, \epsilon, t) = \frac{1}{\sqrt{\bar{\alpha}_t}} \left(x_t - \frac{\beta_t}{\sqrt{1 - \bar{\alpha}_t}} \cdot \epsilon \right) \quad (11)$$

With all the components in place, we construct our full inference algorithm, as shown in Algorithm 1, for enhancing low-field samples to their high-field counterparts. We use $J = 3$ for the refinement loop of the algorithm.

3 Experiments and Results

We evaluated our method on the hidden validation set of the challenge by submitting enhanced pseudo high-field images generated from the corresponding low-field inputs. All performance metrics, unless otherwise stated, were computed by the challenge organizers. For all models, intensities of the input volumes were normalized to the range $[-1, 1]$.

Algorithm 1: Inference algorithm used. In succession the bridging and then the denoising diffusion produces the pseudo high-field sample \hat{x}_0^{HF} .

```

 $\epsilon_K \sim \mathcal{N}(0, 1);$ 
 $x_K^{LF} \leftarrow \text{AddNoise}(x_0^{LF}, \epsilon_K, K);$ 
 $\hat{x}_K^{HF} \leftarrow x_K^{LF} + \phi_{\text{bridge}}(x_K^{LF});$ 
 $\hat{x}_0^{HF} \leftarrow \text{RemoveNoise}(\hat{x}_K^{HF}, \epsilon_K, K);$ 
for  $i = K, \dots, 1$ , do
   $\epsilon_i \sim \mathcal{N}(0, 1);$ 
  for  $j = J, \dots, 1$  do
     $\hat{x}_i^{HF} \leftarrow \text{AddNoise}(\hat{x}_0^{HF}, \epsilon_i, i);$ 
     $\hat{x}_0^{HF} \leftarrow \text{RemoveNoise}(\hat{x}_i^{HF}, \epsilon_\theta(\hat{x}_i^{HF}, i), i);$ 
return  $\hat{x}_0^{HF}$ 

```

3.1 Model Training

We trained our denoising diffusion model solely on high-field images. We combine all three contrasts along the channel dimension, enabling cross-contrast learning. The network architecture follows the U-Net design proposed by Karras et al. with [22]. We extended this network to work with 3D convolutions. This network was trained using the AdamW [23] optimizer with a learning rate of 0.0003. We used 3D patches of size (128, 128, 32) for training. Since the high-field images from the hidden validation set were not available, we report performance on an internal test set of 5 scans. Using our proposed inference strategy, the model achieved an SSIM of 0.91 and a PSNR of 30.12 dB. These values represent the upper bound of achievable quality for our full pipeline since, this level simulates an ideal bridge as we stay in the high-field domain.

We trained the bridge network using the Swin UNETR [24] architecture, focusing on noise levels between timesteps 250 and 750 (out of 1000). We choose this wider spectrum both as a method for better generalization and to give us the room to alter the bridging point later on in the pipeline. For the final pipeline, we selected $K = 400$ as the bridging timestep. At this level, the bridge model achieved an average MSE of 0.05 between predicted and ground truth noisy high-field samples in our internal test set, indicating better latent space alignment under noise, since without the bridge model this average is 0.32.

3.2 Low-Field Enhancement

We combined the trained bridge network and high-field diffusion model to perform full enhancement of low-field MR images. The model produced pseudo high-field outputs from the low-field validation set samples, which were evaluated by the challenge organizers. Our model operated on 3D patches of size (128, 128, 32), using a sliding window inference with an overlap of 0.7. Our method achieved an SSIM of 0.779 and a PSNR of 22.85 dB on the hidden validation set. This con-

firmed that the bridged diffusion approach significantly narrows the gap between low and high-field quality. An example of this is shown in Figure 3.

3.3 Ablation Study

We conducted an ablation study to evaluate the contribution of each component:

1. Neither diffusion nor bridge model: Using low-field samples as high-field samples. Assuming $x_0^{LF} \approx x_0^{HF}$.
2. No diffusion model: Applying the bridge, removing the added noise perfectly. Given ϵ_K added to x_0^{LF} to make x_K^{LF} , we remove ϵ_K from $\phi_{\text{bridge}}(x_K^{LF})$ without any diffusion.
3. No bridge model: Assuming $x_K^{LF} \approx x_K^{HF}$. Using the diffusion network to denoise x_K^{LF} .
4. Full pipeline: As described in Algorithm 1.

The results as calculated by the organizers are listed in Table 1.

Model	Component		Metrics			
	Bridge	Diffusion	SSIM	PSNR	MAE	NMSE
1			0.569	17.544	0.072	0.234
2	✓		0.756	22.712	0.036	0.072
3		✓	0.601	17.602	0.07	0.231
4	✓	✓	0.779	22.85	0.034	0.070

Table 1. Ablation study showing the contribution of various components. All metrics are calculated by the challenge organizers on the secret validation set.

4 Discussion and Conclusion

We presented a bridged denoising diffusion model that enhances low-field MR images by explicitly aligning their noisy representations with those of high-field images. By introducing a bridge network at a specific diffusion timestep, we enable a denoising diffusion model to effectively process low-field inputs into pseudo high-field outputs. Our ablation study shows that both the bridge and the diffusion components contribute: the bridge improves latent alignment, while the diffusion model provides high-quality reconstruction. Their combination leads to the highest performance. However, we observe that the contribution of the denoising diffusion model is relatively small compared to the bridge model. Further improvements in this regard should be made.

While our method relies on paired training data, future work could explore semi-supervised or unpaired approaches for broader applicability and data availability. Overall, our framework offers an effective solution for low-field MRI enhancement.

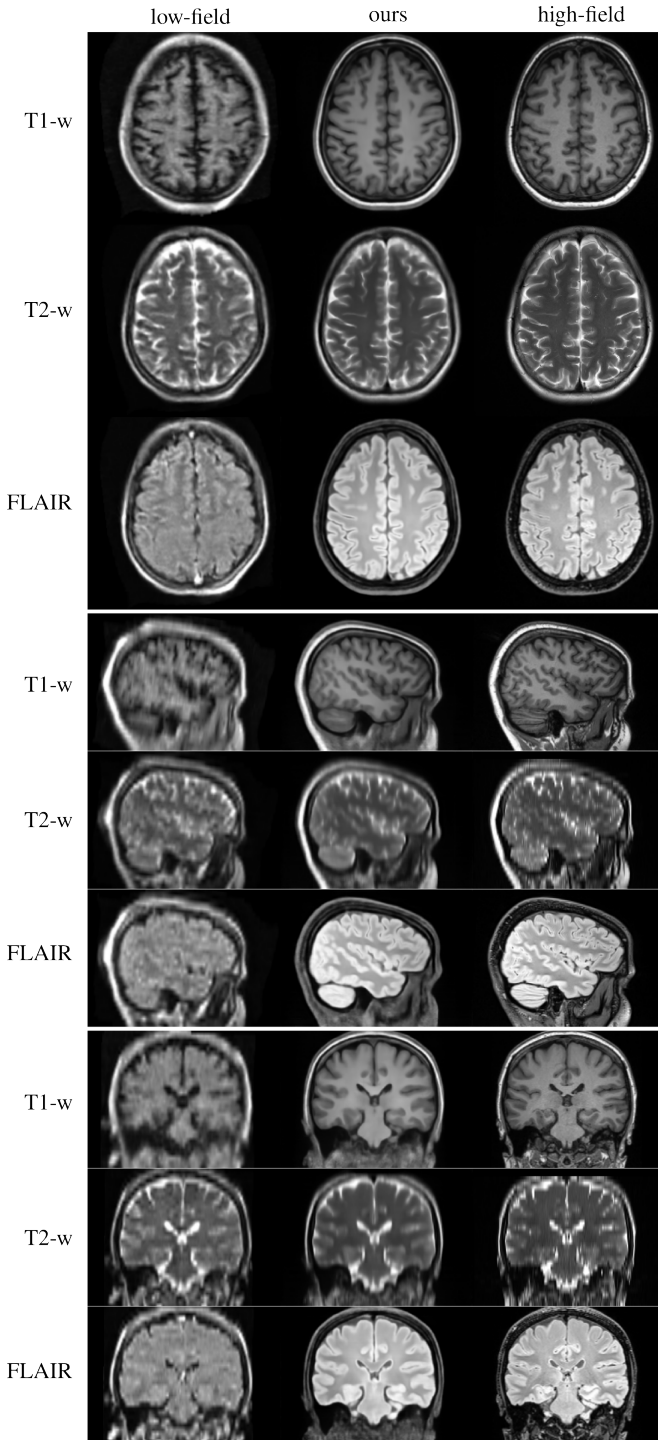


Fig. 3. Example result of the low-field enhancement. From left to right, low-field, pseudo high-field, and the ground truth high-field sample. Three views of the same scan are presented in all three contrasts.

References

1. Dayarathna, S. *et al.* Deep learning based synthesis of MRI, CT and PET: Review and analysis. *Medical Image Analysis* **92**, 103046. ISSN: 1361-8415. <http://dx.doi.org/10.1016/j.media.2023.103046> (Feb. 2024).
2. Sarracanie, M. & Salameh, N. Low-Field MRI: How Low Can We Go? A Fresh View on an Old Debate. *Frontiers in Physics* **8**. ISSN: 2296-424X. <http://dx.doi.org/10.3389/fphy.2020.00172> (June 2020).
3. Arnold, T. C., Freeman, C. W., Litt, B. & Stein, J. M. Low-field MRI: Clinical promise and challenges. en. *Journal of Magnetic Resonance Imaging* **57**, 25–44. ISSN: 1053-1807, 1522-2586. <https://onlinelibrary.wiley.com/doi/10.1002/jmri.28408> (Jan. 2023).
4. Webb, A. & O'Reilly, T. Tackling SNR at low-field: a review of hardware approaches for point-of-care systems. *Magnetic Resonance Materials in Physics, Biology and Medicine* **36**, 375–393. ISSN: 1352-8661. <https://link.springer.com/10.1007/s10334-023-01100-3> (3 May 2023).
5. Guallart-Naval, T. *et al.* Portable magnetic resonance imaging of patients indoors, outdoors and at home. *Scientific Reports* **12**, 13147. ISSN: 2045-2322. <https://www.nature.com/articles/s41598-022-17472-w> (1 July 2022).
6. Deoni, S. C. *et al.* Neuroimaging and verbal memory assessment in healthy aging adults using a portable low-field MRI scanner and a web-based platform: results from a proof-of-concept population-based cross-section study. *Brain Structure and Function* **228**, 493–509. ISSN: 18632661 (2 Mar. 2023).
7. Yuen, M. M. *et al.* Portable, low-field magnetic resonance imaging enables highly accessible and dynamic bedside evaluation of ischemic stroke. *Science Advances* **8**, 3952. ISSN: 2375-2548. <https://www.science.org/doi/10.1126/sciadv.abm3952> (16 Apr. 2022).
8. Arnold, T. C. *et al.* Sensitivity of portable low-field magnetic resonance imaging for multiple sclerosis lesions. *NeuroImage: Clinical* **35**, 103101. ISSN: 22131582. <https://linkinghub.elsevier.com/retrieve/pii/S2213158222001668> (Jan. 2022).
9. Okar, S. V. *et al.* Portable ultra-low-field MRI for progressive multifocal leukoencephalopathy: Case studies, sensitivity, and potential applications. *Journal of Neurology* **272**, 193. ISSN: 0340-5354. <https://link.springer.com/10.1007/s00415-025-12938-z> (3 Mar. 2025).
10. Rowand, E., Owusu, R., Sibole, A., Abu-Haydar, E. & Delarosa, J. Feasibility and Usability of Low-Field Magnetic Resonance Imaging for Pediatric Neuroimaging in Low- and Middle-Income Countries: A Qualitative Study. *Medical Devices: Evidence and Research Volume* **18**, 107–121. ISSN: 1179-1470. <https://www.dovepress.com/feasibility-and-usability-of-low-field-magnetic-resonance-imaging-for-peer-reviewed-fulltext-article-MDER> (Feb. 2025).
11. Islam, K. T. *et al.* Improving portable low-field MRI image quality through image-to-image translation using paired low- and high-field images. *Scienc-*

- tific Reports* **13**. ISSN: 2045-2322. <http://dx.doi.org/10.1038/s41598-023-48438-1> (Dec. 2023).
- 12. Lin, H. *et al.* Low-field magnetic resonance image enhancement via stochastic image quality transfer. *Medical Image Analysis* **87**, 102807. ISSN: 1361-8415. <http://dx.doi.org/10.1016/j.media.2023.102807> (July 2023).
 - 13. Chung, H. & Ye, J. C. Score-based diffusion models for accelerated MRI. *Medical Image Analysis* **80**, 102479. ISSN: 1361-8415. <http://dx.doi.org/10.1016/j.media.2022.102479> (Aug. 2022).
 - 14. Dayarathna, S. *et al.* *McCaD: Multi-Contrast MRI Conditioned, Adaptive Adversarial Diffusion Model for High-Fidelity MRI Synthesis in 2025 IEEE/CVF Winter Conference on Applications of Computer Vision (WACV)* (IEEE, Feb. 2025), 670–679. <http://dx.doi.org/10.1109/WACV61041.2025.00075>.
 - 15. Lin, X. *et al.* in *Medical Image Computing and Computer Assisted Intervention – MICCAI 2024* 775–785 (Springer Nature Switzerland, 2024). ISBN: 9783031721045. http://dx.doi.org/10.1007/978-3-031-72104-5_74.
 - 16. Dayarathna, S., Islam, K. T. & Chen, Z. *Ultra Low-Field to High-Field MRI Translation Using Adversarial Diffusion* in *2024 IEEE International Symposium on Biomedical Imaging (ISBI)* (2024), 1–4.
 - 17. Wang, Z., Bovik, A., Sheikh, H. & Simoncelli, E. Image quality assessment: from error visibility to structural similarity. *IEEE Transactions on Image Processing* **13**, 600–612 (2004).
 - 18. Ho, J., Jain, A. & Abbeel, P. *Denoising Diffusion Probabilistic Models* 2020. <https://arxiv.org/abs/2006.11239>.
 - 19. Kanopoulos, N., Vasanthavada, N. & Baker, R. Design of an image edge detection filter using the Sobel operator. *IEEE Journal of Solid-State Circuits* **23**, 358–367 (1988).
 - 20. Zhao, K., Hung, A. L. Y., Pang, K., Zheng, H. & Sung, K. *PartDiff: Image Super-resolution with Partial Diffusion Models* 2023. <https://arxiv.org/abs/2307.11926>.
 - 21. Chung, H. & Ye, J. C. *Score-based diffusion models for accelerated MRI* 2021. <https://arxiv.org/abs/2110.05243>.
 - 22. Karras, T. *et al.* *Analyzing and Improving the Training Dynamics of Diffusion Models* 2023. <https://arxiv.org/abs/2312.02696>.
 - 23. Loshchilov, I. & Hutter, F. *Decoupled Weight Decay Regularization* 2017. <https://arxiv.org/abs/1711.05101>.
 - 24. Hatamizadeh, A. *et al.* *Swin UNETR: Swin Transformers for Semantic Segmentation of Brain Tumors in MRI Images* 2022. <https://arxiv.org/abs/2201.01266>.